Journal of the Korean Physical Society (2023) 82:1047–1054
https://doi.org/10.1007/s40042-023-00756-3

Online ISSN 1976-8524
Print ISSN 0374-4884

ORIGINAL PAPER - ATOMS, MOLECULES AND OPTICS

Ultra-broadband and flexible metamaterial absorber based on MoS_2 cuboids with Mie resonances

Duong Thi Ha[1,2,3] · Man Hoai Nam[1,2] · Bui Son Tung[1,2] · Bui Xuan Khuyen[1,2] · Vu Dinh Lam[2] · Quynh Le-Van[4]

Received: 19 October 2022 / Revised: 9 January 2023 / Accepted: 3 February 2023 / Published online: 2 March 2023
© The Korean Physical Society 2023

Abstract
In this work, we present a type of flexible and broadband metamaterial absorber operating in the GHz range. The proposed structure consists of three layers: a periodic square-shaped array made of molybdenum disulfide (MoS_2) on the top, a continuous polyimide layer in the middle and a continuous copper layer at the bottom. For flat model, the proposed absorber exhibits a broadband absorption in the frequency range of 10.1–17.6 GHz with an absorption of more than 90% under normal incidence. Due to the symmetry of structure, the absorption feature is polarization-insensitive. The absorption remains above 80% in the frequency range of 11.1–15.6 GHz when the incident angle is up to 60° for TE-polarized wave, while the absorption is higher than 90% in the frequency range of 13.5–18 GHz for incident angles up to 60° for TM-polarized wave. For bending model, the absorption is significantly expanded when the bending radius decreases to under 100 mm. The physical mechanism of the absorption properties is explained in detail by the electric field distribution, the magnetic field distribution following the Mie resonance theory and influence of the loss of MoS_2. Obtained results in the work might contribute to the development of potential applications based on metamaterials in the microwave region such as imaging, protecting and light emitting devices.

Keywords Metamaterial absorber · MoS_2 material · Mie resonances

1 Introduction

Metamaterial absorber (MA) was the firstly introduced by Landy et al. in 2008 [1], and it consists of three layers, including two metallic elements separated by a dielectric spacer. This absorber could achieve an absorption of 96%, while the total thickness of MA was only 1/30 of the working wavelength. Since then, MAs have gained a huge attention of researchers and have been studied for various applications including sensors [2–7], imaging [8–10], energy harvesting [11, 12], stealth technology [13, 14] and light emitting diode [15]. Generally, MAs can overcome the drawbacks of conventional absorbers, and the size and weight of absorbers are reduced, while absorption performance is increased.

To make MAs become more usable in practical applications, especially in the wireless communication and stealth technology, MAs must be designed to attain large operational bandwidth. Therefore, several methods have been introduced to broaden the bandwidth of MAs. One of the popular methods employed in expanding the bandwidth of MAs is to combine various resonance peaks together. In this approach, MAs are composed of multi-resonance units with different size/shapes in a single-layer or are designed as a multilayer structure [16–18]. For example, Ma et al. obtained a broadband metamaterial absorber operating in the mid-infrared range using multiplexed cross resonators. The unit cell was constructed from four different size crosses and

✉ Bui Son Tung
tungbs@ims.vast.ac.vn

✉ Bui Xuan Khuyen
khuyenbx@ims.vast.ac.vn

✉ Vu Dinh Lam
lamvd@gust-edu.vast.vn

[1] Institute of Materials Science, Vietnam Academy of Science and Technology, 18 Hoang Quoc Viet, Hanoi 100000, Vietnam

[2] Graduate University of Science and Technology, Vietnam Academy of Science and Technology, 18 Hoang Quoc Viet, Hanoi 100000, Vietnam

[3] Thai Nguyen University of Education, Thai Nguyen 250000, Vietnam

[4] College of Engineering and Computer Science, VinUniversity, Gia Lam District, Hanoi 14000, Vietnam

as a result, the four peaks are very close together and overlap to form a wide absorption band [19]. Ding et al. designed an ultra-broadband metamaterial absorber that was composed of a periodic array of quadrangular frustum pyramids, in which each pyramid contained 20 stacked metallic–dielectric pairs. This structure reached broadband absorption with nearly unity absorption from 8 to 14 GHz [20]. Although this approach has been demonstrated to be effective in generating wideband absorbers, it requires a large unit volume as well as complex processing. To overcome this challenging, the lumped resistors have been exploited to obtain broadband metamaterial absorbers [21–24]. Despite the compact structure, integrating lumped resistors to the structure surface make it difficult to fabricate, especially in large-scale fabrication.

Recently, molybdenum disulfide (MoS_2) has become one of the most widely studied transition metal dichalcogenides. Due to its unique electrical and optical properties, MoS_2 is a promise candidate for microwave absorbers [25–28]. It is noteworthy that integrating monolayer MoS_2 into metamaterials can expand the operating bandwidth in the infrared and visible range [29–33]. For instance, Huo et al. presented a broadband perfect absorber with monolayer MoS_2 and hexagonal titanium nitride nanodisk array, which showed an average absorption of 98.1% over the entire visible regime from 400 to 850 nm [34]. Sun et al. showed that a universal configuration consisting of monolayer MoS_2 and the silver–insulator–silver structure can obtain broadband and highly efficient absorption [35]. However, to the best of our knowledge, related research on MoS_2-based metamaterial absorbers operating in the GHz range has been rarely reported.

In this paper, we propose a simple design of flexible broadband metamaterial absorber based on MoS_2 in the GHz region. The proposed structure consists of three layers, MoS_2–polyimide–copper, that perform as a broadband absorber with absorption above 90% covering the region of 7.5 GHz from 10.1 to 17.6 GHz. In addition, the absorption bandwidth of bending MA is broader than that of flat MA, making the proposed MA more feasible for real applications.

2 Structure design and methods

A schematic of the proposed MA with optimized unit cell is illustrated in Fig. 1. The structure consists of three layers, in which a square-shaped MoS_2 block is placed on the top, the middle layer is made of polyimide with a thickness of t_s, and the bottom is a continuous copper plate. In our simulation, we took the relative permittivity of polyimide to be 3.5 with a loss tangent of 0.0027 and the thickness of the copper layer was chosen to be $t_m = 0.035\,mm$ with a conductivity of $5.8 \times 10^7 S/m$. The MoS_2 material, whose

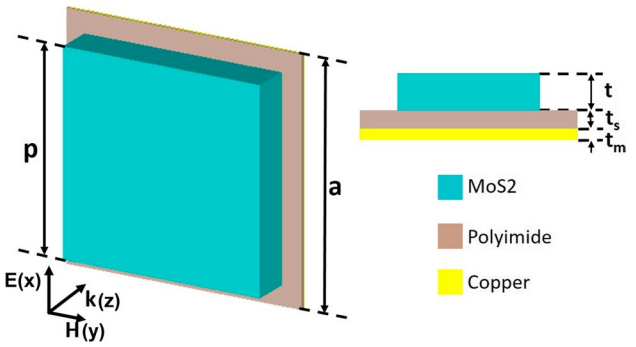

Fig.1 Schematic of the unit cell of the proposed MA with $a = 18$, $t_s = 0.25$, $t = 3$, $t_m = 0.035$, and $p = 15$ mm

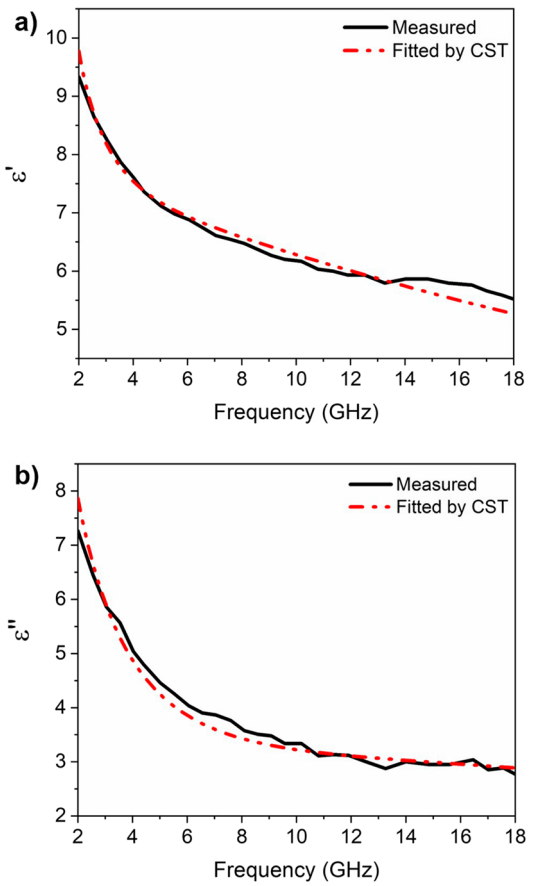

Fig. 2 Complex permittivity of MoS_2: **a** the real part (ε′) and **b** the imaginary part (ε″). The measured permittivity is employed from Ref. 36

frequency-dependent complex permittivity was measured by Wang et al. [36] as indicated in Fig. 2, is employed as a dielectric resonance structure with a size of p and thickness of t in our design. The geometrical parameters are optimized to be $a = 18$, $t_s = 0.25$, $t = 3$ and $p = 15mm$.

Our simulations were carried out using the CST Microwave Studio software [37]. The frequency domain solver is used with a frequency range from 8.0 to 18 GHz. The periodic boundary conditions are used in the x- and y-directions. The absorption is calculated by $A(\omega) = 1 - R(\omega) - T(\omega)$, in which $R(\omega) = |S_{11}(\omega)|^2$ and $T(\omega) = |S_{21}(\omega)|^2$ are reflection and transmission, respectively. In our design, the bottom layer is continuous copper plate; therefore, the transmission is vanished, and the absorption becomes $A(\omega) = 1 - R(\omega)$.

The proposed structure can be fabricate using screen stencil method. Firstly, MoS_2 material is obtained via a hydrothermal preparation, as presented in Ref. [36]. Secondly, to make patterns on polyimide substrate, a stencil will be fabricated with the air holes are designed as the cuboid array in Fig. 1 and placed on the substrate. Then, the ready-made MoS_2 material will be transferred to the substrate by spraying. This step can be repeated several times to obtain the MoS_2 layer with the desired thickness. Finally, the stencil will be removed, and the designed patterns will be left on the polyimide substrate.

3 Results and discussion

Firstly, we investigated the absorption characteristics of the MoS_2 material, which is exploited on a copper plate (Fig. 3a). The thickness of the MoS_2 layer is $t = 3mm$, and the copper plate thickness is $t_m = 0.035mm$. In this simulation, the complex permittivity of MoS_2 depends on the frequency, as illustrated in Fig. 2. The absorption spectrum of copper-backed

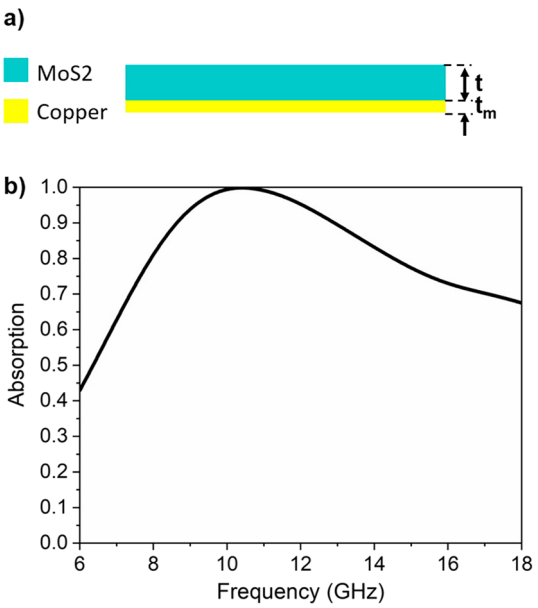

Fig. 3 **a** Schematic of the copper-backed MoS_2 structure and **b** the corresponding absorption spectrum

MoS_2 is simulated and presented in Fig. 3b. It is evident that the copper-backed MoS_2 can be referred to as an absorber with an absorption higher than 90% in a frequency of 4.2 GHz (from 8.6 GHz to 12.8 GHz). Our simulated result is in accordance with the reported result in Ref. [36]. The fractional bandwidth (FBW) of absorption spectrum is also calculated using the following equation:

$$FBW = 2\frac{f_{high} - f_{low}}{f_{high} + f_{low}} \tag{1}$$

where f_{high} and f_{low} are the highest and lowest frequencies where the absorption intensity is greater than 90%, respectively. According to Eq. (1), the FBW of the copper-backed MoS_2 is approximately 39%.

To improve the absorption characteristic, we study the absorption of a MA based on MoS_2 material in which the unit cell is constructed as presented in Fig. 1. For the flat MA model, we simulated the absorption spectrum at normal incidence. The result in Fig. 4a indicates that our structure acts as a broadband absorber with absorption above 90% in a frequency range from 10.1 GHz to 17.6 GHz. Calculation results show that our MA achieves a high-absorption performance with an FBW of 54.15% in the planar configuration. In comparison with the absorption of copper-backed MoS_2, it can be seen that, by integrating MoS_2 material into the MA structure, the absorption spectrum is significantly expanded, from 4.2 GHz to 7.5 GHz for conventional copper-backed MoS_2 and MoS_2-based MA, respectively. Figure 4b presents the ratio of the percentage of energy dissipated in different parts to the total captured power of the MA structure. It is evident that the loss in the MoS_2 cuboids is dominant (nearly 100%), while in the dielectric part is limited to 0.05%.

In our simulation, MoS_2 cuboids is defined as a dielectric material; thus, the electromagnetic characteristics of proposes MA structure can be described on the basis of the Mie resonance theory, which is relevant to the interaction between EM waves and dielectric particles. According to the scattering theory, the scattered EM waves can be depicted by the effective permittivity and permeability. For a spherical dielectric block with radius r and refractive index n, the scattered fields can be represented by a series of 2 m-pole terms of the scattered electric and magnetic field [38], which proportion to:

$$a_m = \frac{n\psi_m(nx)\psi'_m(x) - \psi_m(x)\psi'_m(nx)}{n\psi_m(nx)\xi'_m(x) - \xi_m(x)\psi'_m(nx)} \tag{2}$$

$$b_m = \frac{\psi_m(nx)\psi'_m(x) - n\psi_m(x)\psi'_m(nx)}{\psi_m(nx)\xi'_m(x) - n\xi_m(x)\psi'_m(nx)} \tag{3}$$

where $x = k_0 x_0$, k_0 is the free-space wavenumber, and $\psi_m(x)$ and $\xi_m(x)$ are the Riccati–Besel functions. a_m relates to the electric, and b_m relates to magnetic responses of the sphere.

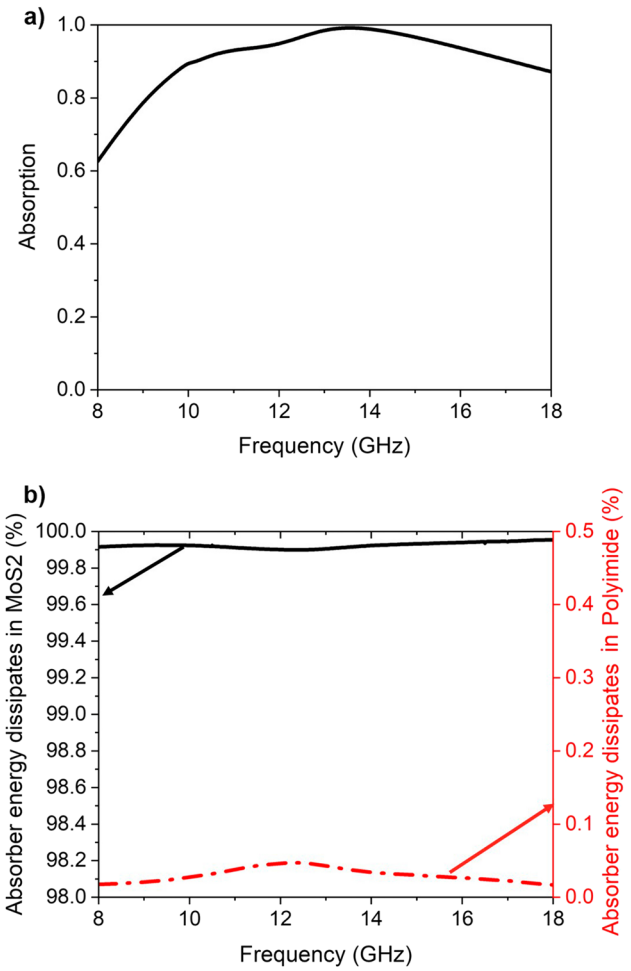

Fig. 4 **a** Absorption spectra of the designed MA structure and **b** the captured energy dissipated in MoS_2 and polyimide of the MA structure

Using Mie theory, the electric dipole coefficient a_1 and the magnetic dipole magnetic coefficient b_1 corresponding to the lowest resonant frequencies can be estimated, and the sphere acts as electric and magnetic dipoles [38].

To gain insights into the absorption mechanism, the distributions of the electric and magnetic fields are simulated at the two frequencies of 11.7 GHz and 15.3 GHz, which are corresponding to two peaks in the absorption spectrum of MA. The TE polarization wave propagates along the z axis, with the magnetic field and electric field polarized along the x and y axis, respectively. Figure 5a and Fig. 5b show the distributions of electric filed in the y–o–z plane and magnetic field in the x–o–z plane at different frequencies, respectively. At 11.7 GHz, an annular electric field is created, inducing a strong localized magnetic dipole in the MoS_2 cuboid. Reversely, at 15.3 GHz, a strong localized electric dipole is observed owing to a surrounding magnetic field in the cuboid. Therefore, it can be concluded that the first and second Mie resonances are corresponding to the TE_{011} and TM_{011} modes, respectively [39]. Our results are consistent with previous works on dielectric left-hand material [39–43] as expected from Mie resonance theory, each dielectric particle is equivalent to a magnetic dipole near the first resonant mode with lower frequency and to an electric dipole near the second resonance mode with higher frequency [44]. From this point, we can conclude that the broad bandwidth of our structure is achieved by a combination of two Mie resonance modes, TE_{011} and TM_{011}.

To gain insights into the role of the imaginary part of complex dielectric constant (ε'') in the broadband mechanism, we study the absorption characteristics of the MA structure with various values of ε'', as shown in Fig. 6. With the initial value of ε'', as depicted in Fig. 2, the absorption spectrum is wide band in which the absorption is greater than 90% in the frequency range from 10.1 to 17.6 GHz. The value of the ε'' is then reduced by a ratio of 1/2, 1/4, 1/6, and 1/8 of the original value. The simulation results show that, when the value of ε'' is reduced, and the absorption spectrum is no longer a wide band but changes to a dual-band. Thus, it can be asserted that the wideband absorption occurs mainly due to the large value of the imaginary part of MoS_2 permittivity, which is consistent to the aforementioned result in Fig. 4b. Consequently, it can be confirmed that the wide band absorption occurs mainly due to two factors: The first one is the excitation of two Mie resonance peaks, and the second one is the high dielectric loss of the MoS_2 material, which widens these two resonance peaks to become the broadband absorption spectrum.

To investigate the influences of incidence and polarization angles on the absorption performance of the suggested MA structure, we simulate the absorption spectra of MA under various incidence and polarization angles. Figure 7a presents the evolution of absorption spectrum as the polarization angle changes from 0 to 80°. Because our structure is designed with highly symmetry, the absorption is nearly unchanged when the polarization angle increases. Figure 7b shows that the absorption of MA is affected by the incident angle, but the high absorption is maintained for large incident angles for both TE and TM polarization. For the TE polarization wave, the absorption of MA slightly reduces when the incidence increases from 0 to 60°. As the incident angle is up to 60°, the absorption is still higher than 80% in the frequency range of 11.1 to 15.6 GHz. The result for TM polarization is presented in Fig. 7c. Obviously, the absorption is higher than 90% in the range of 13.5–18 GHz for incident angles up to 60°. Additionally, the absorption spectrum

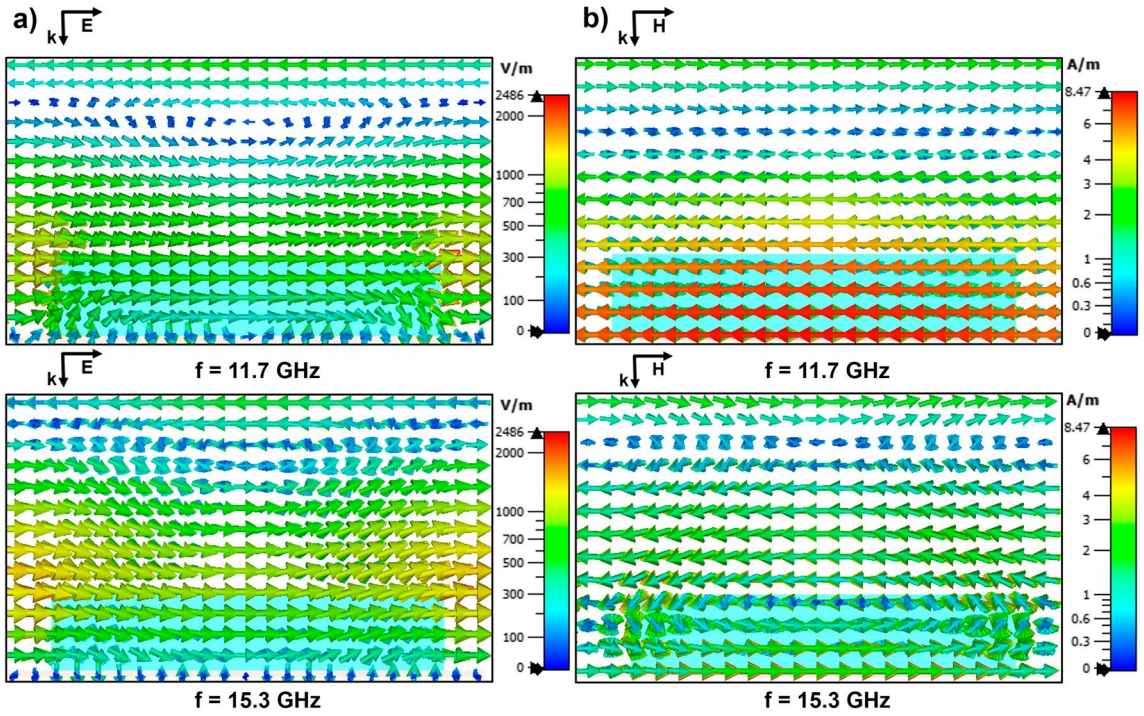

Fig. 5 **a** Electric field and **b** magnetic field distributions at absorption peaks

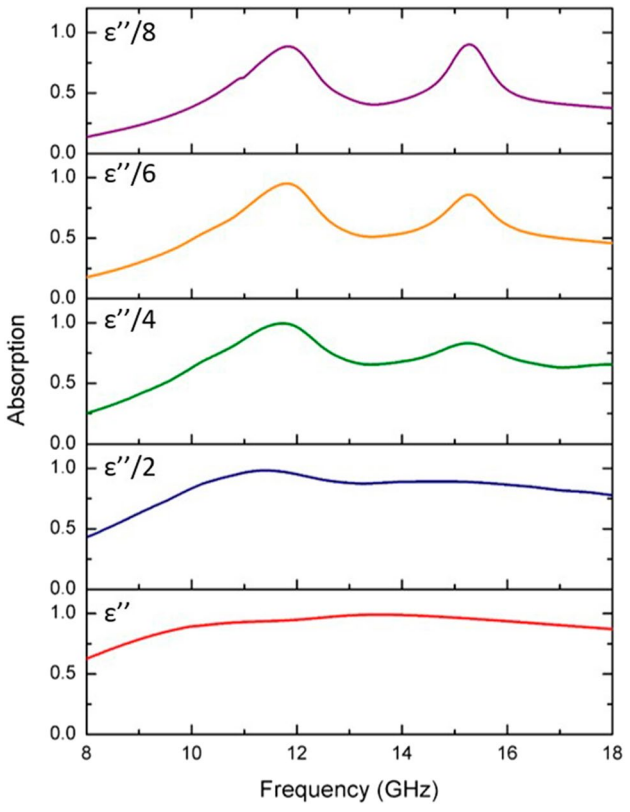

Fig. 6 Absorption spectra of MA corresponding to various imaginary parts of MoS_2 permittivity

is shifted to the higher frequency range and remains broadband. Therefore, it can be concluded that the proposed MA structure is polarization-insensitive and quite stable under oblique incidence.

Our MA structure is composed of resonator units placed on a polyimide dielectric layer; then, it exhibits great flexibility. We investigate the absorption performance of MA when it is bent as a curved model. In this simulation, we construct a full structure and define a bending radius R as indicated in Fig. 8a. Figure 8b shows the simulated absorption for the bent-absorber model with bending radii varying from 500 to 15 mm. One can see that, when $R = 500$ mm, bending structure is nearly planar; thus, the absorption spectra are almost unchanged from the flat model ($R = \infty$). Notably when R decreases from 100 to 20 mm, the absorption spectrum is significantly broadened. At a bending radius of 100 mm, the bent MA absorbs higher than 90% EM waves in the frequency range of 9.5 GHz to 18 GHz, corresponding to an FBW of 61.8%. As the bending radius is reduced to 20 mm, the MA absorption is extended, and absorption above 90% covers the frequency region from 8.3 GHz to 18 GHz, producing FBW reaches 73.7%. However, when the bending radius decreases further to 15 mm, the high-absorption bandwidth is reduced. The influence of bending radius on the FBW of the proposed structure is shown systematically in Fig. 8c. Obviously, the FBW of the proposed MA is kept higher than 54.15% with various R values from

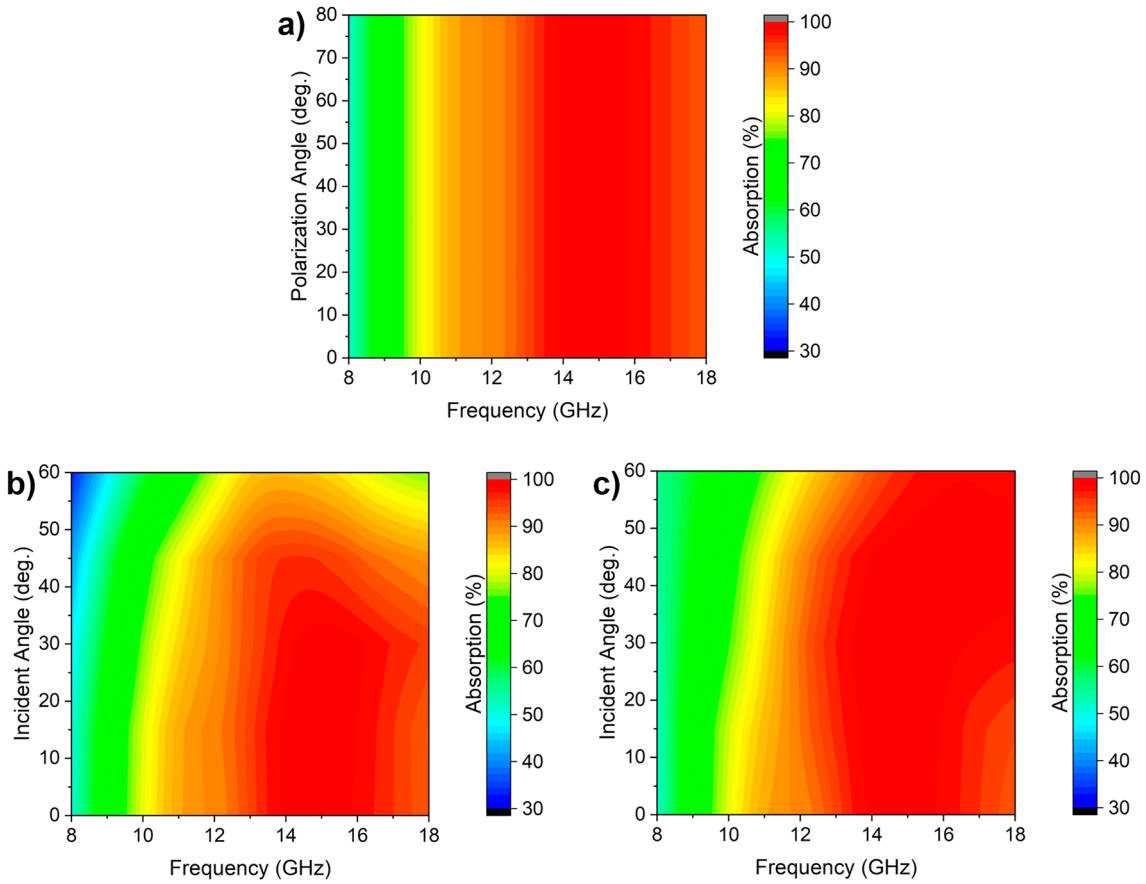

Fig. 7 Dependence of the absorption spectrum of the proposed MA on the **a** polarization angle of normal incidence, **b** incident angle of TE polarization and **c** incident angle of TM polarization

15 to 500 mm. The maximum value FBW is 73.7% corresponding to the radius of 20 mm. The broadening of the absorption spectrum can be explained on the basis of the asymmetry of the structure. When the structure is bent, the EM wave impinges on the surface of the structure at different angles. The electric and magnetic fields distributed on the surface of the material are inhomogeneous (Fig. 8d). As the bending radius decreases, this inhomogeneity increases and will induce new resonances due to the electromagnetic asymmetry of the material. Therefore, as the bending radius decreases, the absorption spectrum of the material is broadened [45, 46].

4 Conclusions

In conclusion, a flexible broadband MA based on MoS_2 material is theoretical studied. A broadband absorption is achieved in the range of 10.1–17.6 GHz with the absorption greater than 90% in the case of normal incidence for all polarization angles. The absorption remains above 80% in the frequency range of 11.1–15.6 GHz at wide incident angles from 0 to 60° for TE polarization, while the absorption is higher than 90% in the range of 13.5–18 GHz for incident angles up to 60° for TM polarization. Additionally, when the MA structure is bent with a bending radius reaching 20 mm, the absorption spectrum is extended in which the above 90% absorption bandwidth covers a range of 9.7 GHz from 8.3 to 18 GHz. The physical mechanism of the proposed MA structure is investigated using electric field and magnetic field distributions, revealing that the high and wide band absorption is governed by Mie resonances and high dielectric loss of MoS_2 material. The results suggest that our designed flexible broadband MA might be suitable for practical applications including flexible stealth systems, electromagnetic shielding, microwave imaging and Meta-LED.

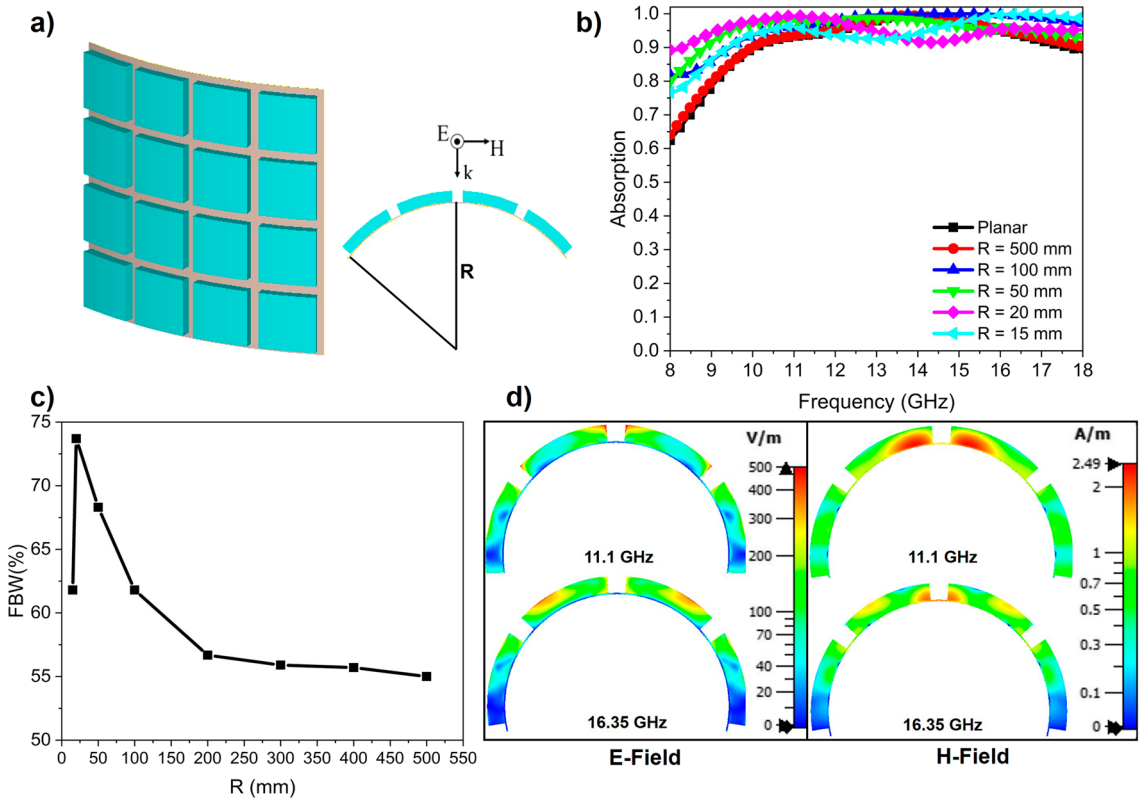

Fig. 8 **a** Definition of bending radius, **b** dependence of the simulated absorption spectrum on bending radius, **c** dependence of the FBW on bending radius and **d** electric and magnetic distributions in the bent structure ($R = 20$ mm) at different frequencies

Acknowledgements This work is funded by VinBigData, Vingroup and supported by Vingroup Innovation Foundation (VINIF) under the project code VINIF.2021.DA00169.

References

1. N.I. Landy, S. Sajuyigbe, J.J. Mock, D.R. Smith, W.J. Padilla, Phys. Rev. Lett. **100**, 207402 (2008)
2. K.V. Sreekanth, Y. Alapan, M. ElKabbash, E. Ilker, M. Hinczewski, U.A. Gurkan, A.D. Luca, G. Strangi, Nat. Mater. **15**, 621–627 (2016)
3. M. Islam, M.T. Islam, B. Bais, S.H. Almalki, H. Alsaif, Sci. Rep. **12**, 1–18 (2022)
4. Y.I. Abdulkarim, L. Deng, H. Luo, S. Huang, M. Karaaslan, O. Altıntaş, M. Bakır, F.F. Muhammadsharif, H.N. Awl, C. Sabah, K.S.L. Al-badri, J. Mater. Res. Technol. **9**, 10291–10304 (2020)
5. M. Karthikeyan, P. Jayabala, S. Ramachandran, S.S. Dhanabalan, T. Sivanesan, M. Ponnusamy, Nanomaterials **12**, 2693 (2022)
6. M.L. Hakim, T. Alam, M.S. Soliman, N.M. Sahar, M.H. Baharuddin, S.H. Almalki, M.T. Islam, Sci. Rep. **12**, 1–18 (2022)
7. Y. Zhang, P. Lin, Y.S. Lin, Nanomaterials **11**, 598 (2021)
8. J.A. Montoya, Z.B. Tian, S. Krishna, W.J. Padilla, Opt. Exp. **25**, 23343–23355 (2017)
9. S. Haxha, F. AbdelMalek, F. Ouerghi, M.D.B. Charlton, A. Aggoun, X.J.S.R. Fang, Sci. Rep. **8**, 1–15 (2018)
10. H. Ahmadi, S. Vaezi, V.J. Harzand, R. Safian, Solid State Commun. **323**, 114023 (2021)
11. X. Xu, Q. Wu, Y. Pang, Y. Cao, Y. Fang, G. Huang, C. Cao, Adv. Funct. Mater. **32**, 2107896 (2022)
12. F.O. Alkurt, O. Altintas, M. Ozakturk, M. Karaaslan, O. Akgol, E. Unal, C. Sabah, Phys. Lett. A **384**, 126041 (2020)
13. K. Iwaszczuk, A.C. Strikwerda, K. Fan, X. Zhang, R.D. Averitt, P.U. Jepsen, Opt. Express **20**, 635–643 (2012)
14. J. Kim, K. Han, J.W. Hahn, Sci. Rep. **7**, 1–9 (2017)
15. W. Chen, J. Zhan, Y. Zhou, R. Chen, Y. Wang, Y. Ma, A.C.S. Appl, Mater. Interfaces **13**, 54497–54502 (2021)
16. Y. Zhou, Z. Qin, Z. Liang, D. Meng, H. Xu, D.R. Smith, Y. Liu, Light Sci. Appl. **10**, 1–12 (2021)
17. B.X. Khuyen, V.T.H. Hanh, B.S. Tung, V.D. Lam, Y.J. Kim, Y. Lee, H.T. Tu, L.Y. Chen, Crystals **10**, 415 (2020)
18. C.M. Tran, H. Van Pham, H.T. Nguyen, T.T. Nguyen, L.D. Vu, T.H. Do, Plasmonics **14**, 1587–1592 (2019)
19. W. Ma, Y. Wen, X. Yu, Opt. Express **21**, 30724–30730 (2013)
20. F. Ding, Y. Cui, X. Ge, Y. Jin, S. He, Appl. Phys. Lett. **100**, 103506 (2012)
21. Y.J. Kim, J.S. Hwang, Y.J. Yoo, B.X. Khuyen, J.Y. Rhee, X. Chen, Y. Lee, J. Phys. D: Appl. Phys. **50**, 405110 (2017)
22. T.Q.H. Nguyen, T.K.T. Nguyen, T.N. Cao, H. Nguyen, L.G. Bach, AIP Adv. **10**, 035326 (2020)
23. A.A.G. Amer, S.Z. Sapuan, A. Alzahrani, N. Nasimuddin, A.A. Salem, S.S. Ghoneim, Electronics **11**, 1986 (2022)
24. D.T. Phan, T.K.T. Nguyen, N.H. Nguyen, D.T. Le, X.K. Bui, D.L. Vu, C.L. Truong, T.Q.H. Nguyen, Phys. Status Solidi B **258**, 2100175 (2021)

25. D. Zhang, J. Chai, J. Cheng, Y. Jia, X. Yang, H. Wang, Z. Zhao, C. Han, G. Shan, W. Zhang, G. Zheng, Appl. Surf. Sci. **462**, 872–882 (2018)
26. L. Xu, J. Tao, X. Zhang, Z. Yao, B. Wei, F. Yang, C. Zhou, A. Zavabeti, K. Zuraiqi, J. Zhou, A.C.S. Appl, Nano Mater. **4**, 11199–11209 (2021)
27. L. Vovchenko, L. Matzui, O. Yakovenko, V. Oliynyk, T. Len, A. Naumenko, L. Kulikov, J. Appl. Phys. **131**, 035103 (2022)
28. P. Negi, A. Kumar, Nanoscale Adv. **3**, 4196–4206 (2021)
29. Y. Pei, T. Sang, Q. Mi, J. Wang, Y. Wang, J. Opt. **24**, 024001 (2021)
30. X. Luo, P. Xiang, H. Yu, S. Huang, T. Yu, Y.F. Zhu, IEEE Photonics Technol. Lett. **34**, 1100–1103 (2022)
31. M. Hashemi, N. Ansari, M. Vazayefi, Sci. Rep. **12**, 1–9 (2022)
32. J. Li, Z. Chen, H. Yang, Z. Yi, X. Chen, W. Yao, T. Duan, P. Wu, G. Li, Y. Yi, Nanomaterials **10**, 257 (2020)
33. H. Xu, L. Hu, Y. Lu, J. Xu, Y. Chen, J. Phys. Chem. C **123**, 10028–10033 (2019)
34. D. Huo, J. Zhang, H. Wang, X. Ren, C. Wang, H. Su, H. Zhao, Nanoscale Res. Lett. **12**, 1–8 (2017)
35. Z. Sun, F. Huang, Y. Fu, Appl. Opt. **59**, 6671–6676 (2020)
36. X. Lin, J. Wang, Z. Chu, D. Liu, T. Guo, L. Yang, Z. Huang, S. Mu, S. Li, Chin. Chem. Lett. **31**, 1124–1128 (2020)
37. CST Microwave Studio 2015, License ID: 52856–1. Dassault Systèmes. Available online: http://www.cst.com (accessed on 15 June 2021).
38. C.F. Bohren, D.R. Huffman, *Absorption and scattering of light by small particles* (John Wiley & Sons, New York, 2008)
39. Q. Zhao, L. Kang, B. Du, H. Zhao, Q. Xie, X. Huang, B. Li, J. Zhou, L. Li, Phys. Rev. Lett. **101**, 027402 (2008)
40. J. Wang, Z. Xu, Z. Yu, X. Wei, Y. Yang, J. Wang, S. Qu, J. Appl. Phys. **109**, 084918 (2011)
41. N. Yi, S. Sun, Y. Gao, K. Wang, Z. Gu, S. Sun, Q. Song, S. Xiao, Sci. Rep. **6**, 1–7 (2016)
42. N.V. Dung, B.S. Tung, B.X. Khuyen, Y.J. Yoo, Y. Lee, J.Y. Rhee, V.D. Lam, J. Korean Phys. Soc. **68**, 1008–1013 (2016)
43. L. Li, J. Wang, H. Ma, J. Wang, M. Feng, H. Du, M. Yan, J. Zhang, S. Qu, Z. Xu, Appl. Phys. Lett. **108**, 122902 (2016)
44. A.B. Evlyukhin, C. Reinhardt, A. Seidel, B. S. Luk'yanchuk and B. N. Chichkov, Phys. Rev. **82**, 045404 (2010)
45. J.S. Hwang, Y.J. Kim, Y.J. Yoo, K.W. Kim, J.Y. Rhee, L.Y. Chen, Y.P. Lee, Sci. Rep. **7**, 3559 (2017)
46. V. Aksyuk, B. Lahiri, G. Holland, A. Centrone, Nanoscale **7**, 3634–3644 (2015)

Publisher's Note Springer Nature remains neutral with regard to jurisdictional claims in published maps and institutional affiliations.

Springer Nature or its licensor (e.g. a society or other partner) holds exclusive rights to this article under a publishing agreement with the author(s) or other rightsholder(s); author self-archiving of the accepted manuscript version of this article is solely governed by the terms of such publishing agreement and applicable law.